

# Theory of supercurrent transport in SISFS Josephson junctions

S. V. Bakurskiy,<sup>1,2</sup> N. V. Klenov,<sup>2</sup> I. I. Soloviev,<sup>1</sup> M. Yu. Kupriyanov,<sup>1</sup> and A. A. Golubov<sup>3</sup>

<sup>1</sup>*Skobeltsyn Institute of Nuclear Physics, Lomonosov Moscow State University, Leninskie gory, Moscow 119991, Russian Federation*

<sup>2</sup>*Faculty of Physics, Lomonosov Moscow State University, Leninskie gory, Moscow 119992, Russian Federation*

<sup>3</sup>*Faculty of Science and Technology and MESA+ Institute for Nanotechnology, University of Twente, 7500 AE Enschede, The Netherlands*

(Dated: June 20, 2018)

We present the results of theoretical study of Current-Phase Relations (CPR)  $J_S(\varphi)$  in Josephson junctions of SISFS type, where 'S' is a bulk superconductor and 'IsF' is a complex weak link consisting of a superconducting film 's', a metallic ferromagnet 'F' and an insulating barrier 'I'. At temperatures close to critical,  $T \lesssim T_C$ , calculations are performed analytically in the frame of the Ginsburg-Landau equations. At low temperatures numerical method is developed to solve selfconsistently the Usadel equations in the structure. We demonstrate that SISFS junctions have several distinct regimes of supercurrent transport and we examine spatial distributions of the pair potential across the structure in different regimes. We study the crossover between these regimes which is caused by shifting the location of a weak link from the tunnel barrier 'I' to the F-layer. We show that strong deviations of the CPR from sinusoidal shape occur even in a vicinity of  $T_C$ , and these deviations are strongest in the crossover regime. We demonstrate the existence of temperature-induced crossover between 0 and  $\pi$  states in the contact and show that smoothness of this transition strongly depends on the CPR shape.

PACS numbers: 74.45.+c, 74.50.+r, 74.78.Fk, 85.25.Cp

## I. INTRODUCTION

Josephson structures with a ferromagnetic layer became very active field of research because of the interplay between superconducting and magnetic order in a ferromagnet leading to variety of new effects including the realization of a  $\pi$ -state with phase difference  $\pi$  in the ground state of a junction, as well as long-range Josephson coupling due generation of odd-frequency triplet order parameter<sup>1-3</sup>.

Further interest to Josephson junctions with magnetic barrier is due to emerging possibilities of their practical use as elements of a superconducting memory<sup>4-12</sup>, on-chip  $\pi$ -phase shifters for self-biasing various electronic quantum and classical circuits<sup>13-16</sup>, as well as  $\varphi$ -batteries, the structures having in the ground state phase difference  $\varphi_g = \varphi$ , ( $0 < |\varphi| < \pi$ ) between superconducting electrodes<sup>17-25</sup>. In standard experimental implementations SFS Josephson contacts are sandwich-type structures<sup>26-27</sup>. The characteristic voltage  $V_C = J_C R_N$  ( $J_C$  is critical current of the junction,  $R_N$  is resistance in the normal state) of these SFS devices is typically quite low, which limits their practical applications. In SISFS structures<sup>28-32</sup> containing an additional tunnel barrier I, the  $J_C R_N$  product in a 0-state is increased<sup>9</sup>, however in a  $\pi$ -state  $V_C$  is still too small<sup>33,34</sup> due to strong suppression of the superconducting correlations in the ferromagnetic layer.

Recently, new SISFS type of magnetic Josephson junction was realized experimentally<sup>9-12</sup>. This structure represents a connection of an SIS tunnel junction and an sFS contact in series. Properties of SISFS structures are controlled by the thickness of s layer  $d_s$  and by relation between critical currents  $J_{CSIS}$  and  $J_{CsFS}$  of their SIS and sFS parts, respectively. If the thickness of s-layer  $d_s$  is much larger than its coherence length  $\xi_S$  and  $J_{CSIS} \ll J_{CsFS}$ , then characteristic voltage of an SISFS device is determined by its SIS part and may reach its maximum corresponding to a standard SIS junction. At the same time, the phase difference  $\varphi$  in a ground state of an SISFS junction

is controlled by its sFS part. As a result, both 0- and  $\pi$ -states can be achieved depending on a thickness of the F layer. This opens the possibility to realize controllable  $\pi$  junctions having large  $J_C R_N$  product. At the same time, being placed in external magnetic field  $H_{ext}$  SISFS structure behaves as a single junction, since  $d_s$  is typically too thin to screen  $H_{ext}$ . This provides the possibility to switch  $J_C$  by an external field.

However, theoretical analysis of SISFS junctions was not performed up to now. The purpose of this paper is to develop a microscopic theory providing the dependence of the characteristic voltage on temperature  $T$ , exchange energy  $H$  in a ferromagnet, transport properties of FS and sF interfaces and thicknesses of s and F layers. Special attention will be given to determining the current-phase relation (CPR) between the supercurrent  $J_S$  and the phase difference  $\varphi$  across the structure.

## II. MODEL OF SISFS JOSEPHSON DEVICE

We consider multilayered structure presented in Fig.1a. It consists of two superconducting electrodes separated by complex interlayer including tunnel barrier I, intermediate superconducting s and ferromagnetic F films. We assume that the conditions of a dirty limit are fulfilled for all materials in the structure. In order to simplify the problem, we also assume that all superconducting films are identical and can be described by a single critical temperature  $T_C$  and coherence length  $\xi_S$ . Transport properties of both sF and FS interfaces are also assumed identical and are characterized by the interface parameters

$$\gamma = \frac{\rho_S \xi_S}{\rho_F \xi_F}, \quad \gamma_B = \frac{R_{BF} \mathcal{A}_B}{\rho_F \xi_F}. \quad (1)$$

Here  $R_{BF}$  and  $\mathcal{A}_B$  are the resistance and area of the sF and FS interfaces  $\xi_S$  and  $\xi_F$  are the decay lengths of S and F materials

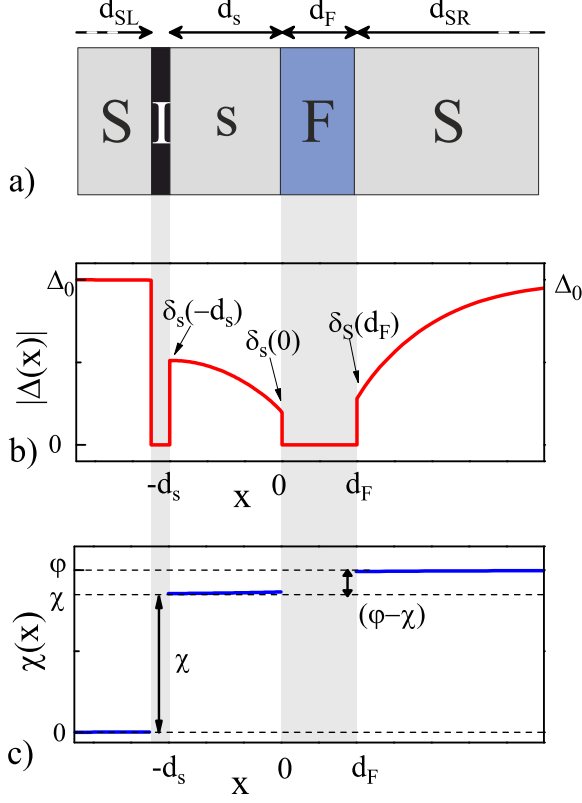


FIG. 1: a) Schematic design of SIFS Josephson junction. b), c) Typical distribution of amplitude  $|\Delta(x)|$  and phase difference  $\chi(x)$  of pair potential along the structure.

while  $\rho_S$  and  $\rho_F$  are their resistivities.

Under the above conditions the problem of calculation of the critical current in the SIFS structure reduces to solution of the set of the Usadel equations<sup>35</sup>. For the S layers these equations have the form<sup>1-3</sup>

$$\frac{\xi_S^2}{\Omega G_m} \frac{d}{dx} \left( G_m^2 \frac{d}{dx} \Phi_m \right) - \Phi_m = -\Delta_m, \quad G_m = \frac{\Omega}{\sqrt{\Omega^2 + \Phi_m \Phi_m^*}}, \quad (2)$$

$$\Delta_m \ln \frac{T}{T_C} + \frac{T}{T_C} \sum_{\omega=-\infty}^{\infty} \left( \frac{\Delta_m}{|\Omega|} - \frac{\Phi_m G_m}{\Omega} \right) = 0, \quad (3)$$

where  $m = S$  for  $x \leq -d_s$  and  $x \geq d_F$ ;  $m = s$  in the interval  $-d_s \leq x \leq 0$ . In the F film ( $0 \leq x \leq d_F$ ) they are

$$\xi_F^2 \frac{d}{dx} \left( G_F^2 \frac{d}{dx} \Phi_F \right) - \tilde{\Omega} \Phi_F G_F = 0. \quad (4)$$

Here  $\Omega = T(2n+1)/T_C$  are Matsubara frequencies normalized to  $\pi T_C$ ,  $\tilde{\Omega} = \Omega + iH/\pi T_C$ ,  $G_F = \tilde{\Omega}/(\tilde{\Omega}^2 + \Phi_{F,\omega} \Phi_{F,-\omega}^*)^{1/2}$ ,  $H$  is exchange energy,  $\xi_{S,F}^2 = (D_{S,F}/2\pi T_C)$

and  $D_{S,F}$ , are diffusion coefficients in S and F metals, respectively. Pair potential  $\Delta_m$  and the Usadel functions  $\Phi_m$  and  $\Phi_F$  in (2) - (4) are also normalized to  $\pi T_C$ . To write equations (2) - (4), we have chosen the  $x$  axis in the directions perpendicular to the SI, FS and sF interfaces and put the origin at sF interface. Equations (2) - (4) must be supplemented by the boundary conditions<sup>36</sup>. At  $x = -d_s$  they can be written as

$$G_S^2 \frac{d}{dx} \Phi_S = G_s^2 \frac{d}{dx} \Phi_s, \quad (5)$$

$$\gamma_{BI} \xi_S G_s \frac{d}{dx} \Phi_s = -G_S (\Phi_S - \Phi_s),$$

where  $\gamma_{BI} = R_{BI} A_B / \rho_S \xi_S$ ,  $R_{BI}$  and  $A_B$  are resistance and area of SI interface. At  $x = 0$  the boundary conditions are

$$\frac{\xi_S}{\Omega} G_s^2 \frac{d}{dx} \Phi_s = \gamma \frac{\xi_F}{\Omega} G_F^2 \frac{d}{dx} \Phi_F, \quad (6)$$

$$\gamma_B \xi_F G_F \frac{d}{dx} \Phi_F = -G_s \left( \frac{\tilde{\Omega}}{\Omega} \Phi_s - \Phi_F \right)$$

and at  $x = d_F$  they have the form

$$\frac{\xi_S}{\Omega} G_s^2 \frac{d}{dx} \Phi_s = \gamma \frac{\xi_F}{\Omega} G_F^2 \frac{d}{dx} \Phi_F, \quad (7)$$

$$\gamma_B \xi_F G_F \frac{d}{dx} \Phi_F = G_s \left( \frac{\tilde{\Omega}}{\Omega} \Phi_s - \Phi_F \right),$$

Far from the interfaces the solution should cross over to a uniform current-carrying superconducting state<sup>37-39</sup>

$$\Phi_S(\mp\infty) = \Phi_\infty \exp \{ i(\chi(\mp\infty) - ux/\xi_S) \}, \quad (8)$$

$$\Delta_S(\mp\infty) = \Delta_0 \exp \{ i(\chi(\mp\infty) - ux/\xi_S) \}, \quad (9)$$

$$\Phi_\infty = \frac{\Delta_0}{1 + u^2 / \sqrt{\Omega^2 + |\Phi_S|^2}}, \quad (10)$$

resulting in order parameter phase difference across the structure equal to

$$\varphi = \varphi(\infty) - 2ux/\xi_S, \quad \varphi(\infty) = \chi(\infty) - \chi(-\infty). \quad (11)$$

Here  $\varphi(\infty)$  is the asymptotic phase difference across the junction,  $\Delta_0$  is modulus of order parameters far from the boundaries of the structure at a given temperature,  $u = 2mv_s \xi_S$ ,  $m$  is the electron mass and  $v_s$  is the superfluid velocity. Note that since the boundary conditions (5) - (6) include the Matsubara frequency  $\Omega$ , the phases of  $\Phi_S$  functions depend on  $\Omega$  and are different from the phase of the pair potential  $\Delta_S$  at the FS interfaces  $\chi(d_F)$  and  $\chi(0)$ . Therefore it is the value  $\varphi(\infty)$  rather than  $\varphi = \chi(d_F) - \chi(0)$ , that can be measured experimentally by using a scheme compensating the linear in  $x$  part in Eq. (11).

The boundary problem (2)-(11) can be solved numerically making use of (8), (10). Accuracy of calculations can be monitored by equality of currents  $J_S$

$$\frac{2eJ_S(\varphi)}{\pi T A_B} = \sum_{\omega=-\infty}^{\infty} \frac{iG_{m,\omega}^2}{\rho_m \Omega^2} \left[ \Phi_{m,\omega} \frac{\partial \Phi_{m,-\omega}^*}{\partial x} - \Phi_{m,-\omega}^* \frac{\partial \Phi_{m,\omega}}{\partial x} \right], \quad (12)$$

calculated at the SI and FS interfaces and in the electrodes.

In the further analysis carried out below we limit ourselves to the consideration of the most relevant case of low-transparent tunnel barrier at SI interface

$$\gamma_{BI} \gg 1. \quad (13)$$

In this approximation, the junction resistance  $R_N$  is fully determined by the barrier resistance  $R_{BI}$ . Furthermore the current flowing through the electrodes can lead to the suppression of superconductivity only in the vicinity of sF and FS interfaces. That means, up to terms of the order of  $\gamma_{BI}^{-1}$  we can neglect the effects of suppression of superconductivity in the region  $x \leq -d_s$  and write the solution in the form

$$\Phi_S(x) = \Delta_S(x) = \Delta_0. \quad (14)$$

Here without any loss of generality we put  $\chi(-\infty) = \chi(-d_s - 0) = 0$  (see Fig. 1c).

Substitution of (14) into boundary conditions (5) gives

$$\gamma_{BI} \xi_S G_s \frac{d}{dx} \Phi_s = - \frac{\Omega}{\sqrt{\Omega^2 + \Delta_0^2}} (\Delta_0 - \Phi_s). \quad (15)$$

Further simplifications are possible in a several limiting cases.

### III. THE HIGH TEMPERATURE LIMIT $T \approx T_C$

In a vicinity of critical temperature the Usadel equations in the F layer can be linearized. Writing down their solution in the analytical form and using the boundary conditions (6), (7) on sF and FS interfaces we can reduce the problem to the solution of Ginzburg-Landau (GL) equations in the s and S layers. We limit our analysis by considering the most interesting case when the following condition is fulfilled:

$$\Gamma_{BI} = \frac{\gamma_{BI} \xi_S}{\xi_S(T)} \gg 1, \quad (16)$$

and when there is strong suppression of superconductivity in the vicinity of the sF and FS interfaces. The latter takes place if the parameter  $\Gamma$

$$\Gamma = \frac{\gamma \xi_S(T)}{\xi_S}, \quad \xi_S(T) = \frac{\pi \xi_S}{2\sqrt{1 - T/T_C}} \quad (17)$$

satisfies the conditions

$$\Gamma p \gg 1, \quad \Gamma q \gg 1. \quad (18)$$

Here

$$p^{-1} = \frac{8}{\pi^2} \text{Re} \sum_{\omega=0}^{\infty} \frac{1}{\Omega^2 \sqrt{\Omega} \coth \frac{d_F \sqrt{\Omega}}{2\xi_F}}, \quad (19)$$

$$q^{-1} = \frac{8}{\pi^2} \text{Re} \sum_{\omega=0}^{\infty} \frac{1}{\Omega^2 \sqrt{\Omega} \tanh \frac{d_F \sqrt{\Omega}}{2\xi_F}}. \quad (20)$$

Note that in the limit  $h = H/\pi T_C \gg 1$  and  $d_F \gg \sqrt{2/h} \xi_F$  the sums in (19), (20) can be evaluated analytically resulting in

$$\beta = \frac{p-q}{p+q} = \sqrt{8} \sin \left( \frac{d_F}{\xi_F} \sqrt{\frac{h}{2}} + \frac{3\pi}{4} \right) \exp \left( -\frac{d_F}{\xi_F} \sqrt{\frac{h}{2}} \right), \quad (21)$$

$$p+q = 2\sqrt{2h}(T/T_C)^2, \quad pq = 2h(T/T_C)^4. \quad (22)$$

In general, the phases of the order parameters in s and S films are functions of the coordinate  $x$ . In the considered approximation the terms that take into account the coordinate dependence of the phases, are proportional to small parameters  $(\Gamma q)^{-1}$  and  $(\Gamma p)^{-1}$  and therefore provide small corrections to the current. For this reason, in the first approximation we can assume that the phases in superconducting electrodes are constants independent of  $x$ . In the further analysis we denote the phases at the s-film by  $\chi$  and at the right S-electrode by  $\varphi$  (see Fig. 1c).

The details of calculations are summarized in the Appendix A. These calculations show that the considered SISFS junction has two modes of operation depending on relation between s layer thickness  $d_s$  and the critical thickness  $d_{sc} = (\pi/2)\xi_S(T)$ . For  $d_s$  larger than  $d_{sc}$ , the s-film keeps its intrinsic superconducting properties (*mode (1)*), while for  $d_s \leq d_{sc}$  superconductivity in the s-film exists only due to proximity effect with the bulk S electrodes (*mode (2)*).

#### A. Mode (1): SIs + sFS junction $d_s \geq d_{sc}$

We begin our analysis with the regime when the intermediate s-layer is intrinsically superconducting. In this case it follows from the solution of GL equations that supercurrent flowing across SIs, sF and FS interfaces ( $J(-d_s)$ ,  $J(0)$  and  $J(d_F)$ , respectively) can be represented in the form (see Appendix A)

$$\frac{J_S(-d_s)}{J_G} = \frac{\delta_s(-d_s)}{\Gamma_{BI} \Delta_0} \sin(\chi), \quad J_G = \frac{\pi \Delta_0^2 \mathcal{A}_B}{4e\rho_S T_C \xi_S(T)}, \quad (23)$$

$$\frac{J_S(0)}{J_G} = \frac{J_S(d_F)}{J_G} = \frac{\Gamma(p-q)}{2\Delta_0^2} \delta_s(0) \delta_S(d_F) \sin(\varphi - \chi), \quad (24)$$

where  $\Delta_0 = \sqrt{8\pi^2 T_C (T_C - T) / 7\zeta(3)}$  is bulk value of order parameter in S electrodes,  $\mathcal{A}_B$  is cross sectional area of the structure,  $\zeta(z)$  is Riemann zeta function. Here

$$\delta_s(0) = \frac{2b(p-q) \cos(\varphi - \chi) - 2a(p+q)}{\Gamma \left[ (p+q)^2 - (p-q)^2 \cos^2(\varphi - \chi) \right]}, \quad (25)$$

$$\delta_S(d_F) = \frac{2b(p+q) - 2a(p-q) \cos(\varphi - \chi)}{\Gamma \left( (p+q)^2 - (p-q)^2 \cos^2(\varphi - \chi) \right)}, \quad (26)$$

are the order parameters at sF and FS interfaces, respectively (see Fig. 1b) and

$$a = -\delta_s(-d_s) \sqrt{1 - \frac{\delta_s^2(-d_s)}{2\Delta_0^2}}, \quad b = \frac{\Delta_0}{\sqrt{2}}, \quad (27)$$

where  $\delta_s(-d_s)$  is the solution of transcendental equation

$$K\left(\frac{\delta_s(-d_s)}{\Delta_0\eta}\right) = \frac{d_s\eta}{\sqrt{2}\xi_S(T)}, \quad \eta = \sqrt{2 - \frac{\delta_s^2(-d_s)}{\Delta_0^2}}. \quad (28)$$

Here,  $K(z)$ , is the complete elliptic integral of the first kind. Substitution of  $\delta_s(-d_s) = 0$  into Eq. (28) leads to the expression for critical s layer thickness,  $d_{sc} = (\pi/2)\xi_S(T)$ , which was used above.

For the calculation of the CPR we need to exclude phase  $\chi$  of the intermediate s layer from the expressions for the currents (23), (24). The value of this phase is determined from the condition that the currents flowing across Is and sF interfaces should be equal to each other.

For large thickness of the middle s-electrode ( $d_s \gg d_{sc}$ ) the magnitude of order parameter  $\delta_s(-d_s)$  is close to that of a bulk material  $\Delta_0$  and we may put  $a = -b$  in Eqs.(25) and (26)

$$\delta_S(d_F) = \delta_S(0) = \frac{\sqrt{2}\Delta_0}{\Gamma((p+q) - (p-q)\cos(\varphi - \chi))}, \quad (29)$$

resulting in

$$J_S(0) = J_S(d_F) = \frac{J_G\beta \sin(\varphi - \chi)}{\Gamma(1 - \beta \cos(\varphi - \chi))} \quad (30)$$

together with the equation to determine  $\chi$

$$\frac{\Gamma}{\Gamma_{BI}} \sin(\chi) = \frac{\beta \sin(\varphi - \chi)}{1 - \beta \cos(\varphi - \chi)}, \quad \beta = \frac{p-q}{p+q}. \quad (31)$$

From (29), (30) and (31) it follows that in this mode SISFS structure can be considered as a pair of SIs and sFS junctions connected in series. Therefore, the properties of the structure are almost independent on thickness  $d_s$  and are determined by a junction with smallest critical current.

Indeed, we can conclude from (31) that the phase  $\chi$  of s layer order parameter depends on the ratio of the critical current,  $I_{CSIs} \propto \Gamma_{BI}^{-1}$ , of its SIs part to that,  $I_{CSFS} \propto |\beta|\Gamma^{-1}$ , of the sFS junction. The coefficient  $\beta$  in (31) is a function of F layer thickness, which becomes close to unity in the limit of small  $d_F$  and exhibits damped oscillations with  $d_F$  increase (see analytical expression for  $\beta$  (21)). That means that there is a range of thicknesses,  $d_{Fn}$ , determined by the equation  $\beta = 0$ , at which  $J_S \equiv 0$  and there is a transition from 0 to  $\pi$  state in sFS part of SISFS junction. In other words, crossing the value  $d_{Fn}$  with an increase of  $d_F$  provides a  $\pi$  shift of  $\chi$  relative to the phase of the S electrode.

In Fig.2 we clarify the classification of operation modes and demonstrate the phase diagram in the  $(d_s, d_F)$  plane, which follows from our analytical results (21)-(28). The calculations have been done at  $T = 0.9T_C$  for  $h = H/\pi T_C = 10$ ,  $\Gamma_{BI} = 200$  and  $\Gamma = 5$ . The structures with s-layer smaller than critical

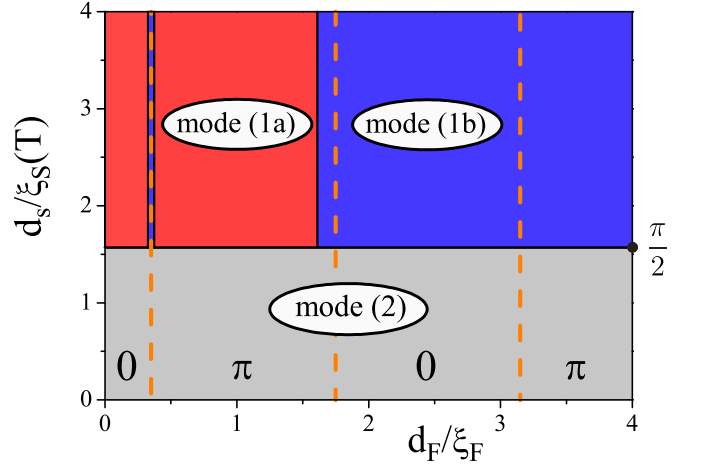


FIG. 2: The phase diagram of the operation modes of the SISFS structure in the  $(d_s, d_F)$  plane. The bottom area corresponds to the *mode (2)* with fully suppressed superconductivity in the s-layer. The top part of the diagram, separated from the bottom one by the solid horizontal line, corresponds to the s-layer in superconductive state. It provides the value of s layer critical thickness,  $d_{sc}$ . The upper-left part indicates the *mode (1a)* with the weak place located at SIs tunnel barrier. The upper-right area as well as thin valley around first  $0 - \pi$  transition correspond to the *mode (1b)* with the weak place located at sFS junction. Solid vertical lines provide loci of the borders between the *modes (1a)* and *(1b)*. Vertical dashed lines show positions of  $0 - \pi$  transitions. The calculations have been done for  $H = 10\pi T_C$ ,  $\Gamma_{BI} = 200$  and  $\Gamma = 5$  at  $T = 0.9T_C$ .

thickness  $d_{sc} = \pi\xi_S(T)/2$  correspond to the *mode (2)* with fully suppressed superconductivity in the s layer. Conversely, the top part of diagram corresponds to s-layer in the superconductive state (*mode (1)*). This area is divided into two parts depending on whether the weak place located at the tunnel barrier I (*mode(1a)*) or at the ferromagnetic F-layer (*mode(1b)*). The separating black solid vertical lines in the upper part in Fig.2 represent the locus of points where the critical currents of SIs and sFS parts of SISFS junction are equal. The dashed lines give the locations of the points of 0 to  $\pi$  transitions,  $d_{Fn} = \pi(n - 3/4)\xi_F\sqrt{2/h}$ ,  $n = 1, 2, 3, \dots$ , at which  $J_S = 0$ . In a vicinity of these points there are the valleys of *mode (1b)* with the width,  $\Delta d_{Fn} \approx \xi_F\Gamma\Gamma_{BI}^{-1}h^{-1/2}\exp\{\pi(n - 3/4)\}$ , embedded into the areas occupied by *mode (1a)*. For the set of parameters used for calculation of the phase diagram presented in Fig.2, there is only one valley with the width  $\Delta d_{F1} \approx \xi_F\Gamma\Gamma_{BI}^{-1}h^{-1/2}\exp\{\pi/4\}$  located around the point  $d_{F1} = (\pi/4)\xi_F\sqrt{2/h}$  of the first 0 to  $\pi$  transition.

### 1. Mode (1a): Switchable $0 - \pi$ SIs junction

In the experimentally realized case<sup>8-11</sup>  $\Gamma_{BI}^{-1} \ll |\beta|\Gamma^{-1}$  the condition is fulfilled and the weak place in SISFS structure is located at the SIs interface. In this approximation it follows from (31) that

$$\chi \approx \varphi - \frac{2q\Gamma}{(p-q)\Gamma_{BI}} \sin(\varphi)$$

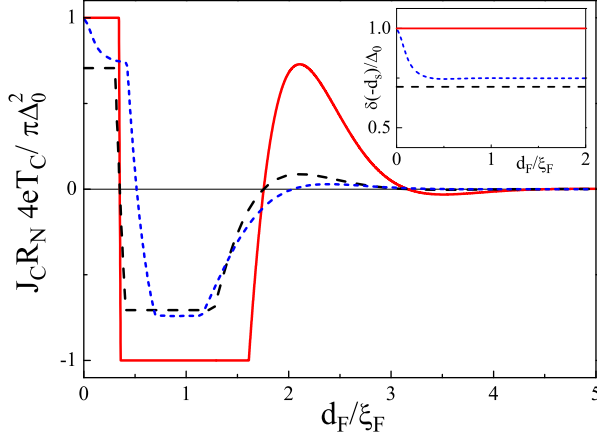


FIG. 3: Critical current  $J_C$  of the SISFS structure versus F-layer thickness  $d_F$  calculated at  $T = 0.9T_C$ ,  $H = 10\pi T_C$ ,  $\Gamma_{BI} = 200$  and  $\Gamma = 5$  for s layer thickness  $d_s = 2\xi_s(T)$  slightly above the critical one  $d_{sc}$ . Inset shows dependence of pair potential  $\delta_s(-d_s)$  at the Is interface of the s-layer versus F-layer thickness  $d_F$ . Solid lines have been calculated for  $d_s \gg d_{sc}$  from Eqs. (32)-(33). The dashed line is the result of calculations using analytical expressions (23)-(28) for the thickness of s-layer  $d_s = 2\xi_s(T)$ . Short-dashed line is the result of numerical calculations in the frame of Usadel equations (2)-(11).

in 0-state ( $d_F < d_{F1}$ ) and

$$\chi \approx \pi + \varphi - \frac{2q\Gamma}{(p-q)\Gamma_{BI}} \sin(\varphi)$$

in  $\pi$ -state ( $d_F > d_{F1}$ ). Substitution of these expressions into (30) results in

$$J_S(\varphi) = \pm \frac{J_G}{\Gamma_{BI}} \left[ \sin \varphi - \frac{\Gamma}{\Gamma_{BI}} \frac{1 \mp \beta}{2\beta} \sin(2\varphi) \right] \quad (32)$$

for 0- and  $\pi$ - states, respectively. It is seen that for  $d_F < d_{F1}$  the CPR (32) has typical for SIS tunnel junctions sinusoidal shape with small correction taking into account the suppression of superconductivity in the s layer due to proximity with FS part of complex sFS electrode. Its negative sign is typical for the tunnel Josephson structures with composite NS or FS electrodes<sup>39,40</sup>. For  $d_F > d_{F1}$  the supercurrent changes its sign thus exhibiting the transition of SISFS junction into  $\pi$  state. It's important to note that in this mode the SISFS structure may have almost the same value of the critical current both in 0 and  $\pi$  states. It is unique property, which can not be realized in SFS devices studied before. For this reason we have identified this mode as "Switchable 0 -  $\pi$  SIS junction".

## 2. Mode (1b): sFS junction

Another limiting case is realized under the condition  $\Gamma_{BI}^{-1} \gg |\beta|\Gamma^{-1}$ . It fulfills in the vicinity of the points of 0- to  $\pi$ -transitions,  $d_{Fn}$ , and for large  $d_F$  values and high exchange fields  $H$ . In this mode (see Fig. 2) the weak place shifts to

sFS part of SISFS device and the structure transforms into a conventional SFS-junction with complex SI electrode.

In the first approximation on  $\Gamma/(\beta\Gamma_{BI}) \gg 1$  it follows from (30), (31) that

$$\chi = \frac{\Gamma_{BI}}{\Gamma} \frac{\beta \sin(\varphi)}{1 - \beta \cos(\varphi)},$$

resulting in

$$J_S(\varphi) = \frac{J_G\beta}{\Gamma(1 - \beta \cos \varphi)} \left( \sin \varphi - \frac{\Gamma_{BI}}{2\Gamma} \frac{\beta \sin(2\varphi)}{(1 - \beta \cos \varphi)} \right). \quad (33)$$

The shape of CPR for  $\chi \rightarrow 0$  coincides with that previously found in SNS and SFS Josephson devices<sup>37</sup>. It transforms to the sinusoidal form for sufficiently large thickness of F layer. For small thickness of the F-layer as well as in the vicinity of 0 -  $\pi$  transitions, significant deviations from sinusoidal form may occurred.

Transition between the *mode (1a)* and the *mode (1b)* is also demonstrated in Fig.3. It shows dependence of critical current  $J_C$  across the SISFS structure versus F-layer thickness  $d_F$ . The inset in Fig.3 demonstrates the magnitude of an order parameter at Is interface as a function of  $d_F$ . The solid lines in Fig.3 give the shape of  $J_C(d_F)$  and  $\delta_0(-d_s)$  calculated from (32)-(33). These equations are valid in the limit  $d_s \gg d_{sc}$  and do not take into account possible suppression of superconductivity in a vicinity of tunnel barrier due to proximity with FS part of the device. The dashed lines are the result of calculations using analytical expressions (23)-(28) for the thickness of the s-layer  $d_s = 2\xi_s(T)$ , which slightly exceeds the critical one,  $d_{sc} = (\pi/2)\xi_s(T)$ . These analytical dependencies are calculated at  $T = 0.9 T_C$  for  $H = 10\pi T_C$ ,  $\Gamma_{BI} = 200$ ,  $\Gamma = 5$ ,  $\gamma_B = 0$ . The short-dashed curves are the results of numerical calculations performed self-consistently in the frame of the Usadel equations (2)-(11) for corresponding set of the parameters  $T = 0.9 T_C$  for  $H = 10\pi T_C$ ,  $\gamma_{BI} = 1000$ ,  $\gamma = 1$ ,  $\gamma_B = 0.3$  and the same thickness of the s layer  $d_{sc} = (\pi/2)\xi_s(T)$ . Interface parameters  $\gamma_{BI} = 1000$ ,  $\gamma = 1$  are chosen the same as for the analytical case. The choice of  $\gamma_B = 0.3$  allows one to take into account the influence of mismatch which generally occurs at the sF and FS boundaries.

It can be seen that there is a qualitative agreement between the shapes of the three curves. For small  $d_F$  the structure is in the 0-state *mode (1a)* regime. The difference between dashed and short dashed lines in this area is due to the fact that the inequalities (18) are not fulfilled for very small  $d_F$ . The solid and short dashed curves start from the same value since for  $d_F = 0$  the sFS electrode becomes a single spatially homogeneous superconductor. For  $d_s = 2\xi_s(T)$  the intrinsic superconductivity in the s layer is weak and is partially suppressed with  $d_F$  increase (see the inset in Fig.3). This suppression is accompanied by rapid drop of the critical current. It can be seen that starting from the value  $d_F \approx 0.4\xi_F$  our analytical formulas (23)-(28) are accurate enough. The larger  $d_s$ , the better agreement between numerical and analytical results due to the better applicability of the GL equations in the s layer. With further  $d_F$  increase the structure passes through the valley of *mode (1b)* state, located in the vicinity of the 0 to  $\pi$  transition, and comes into the  $\pi$ -state of the *mode (1a)*. Finally for

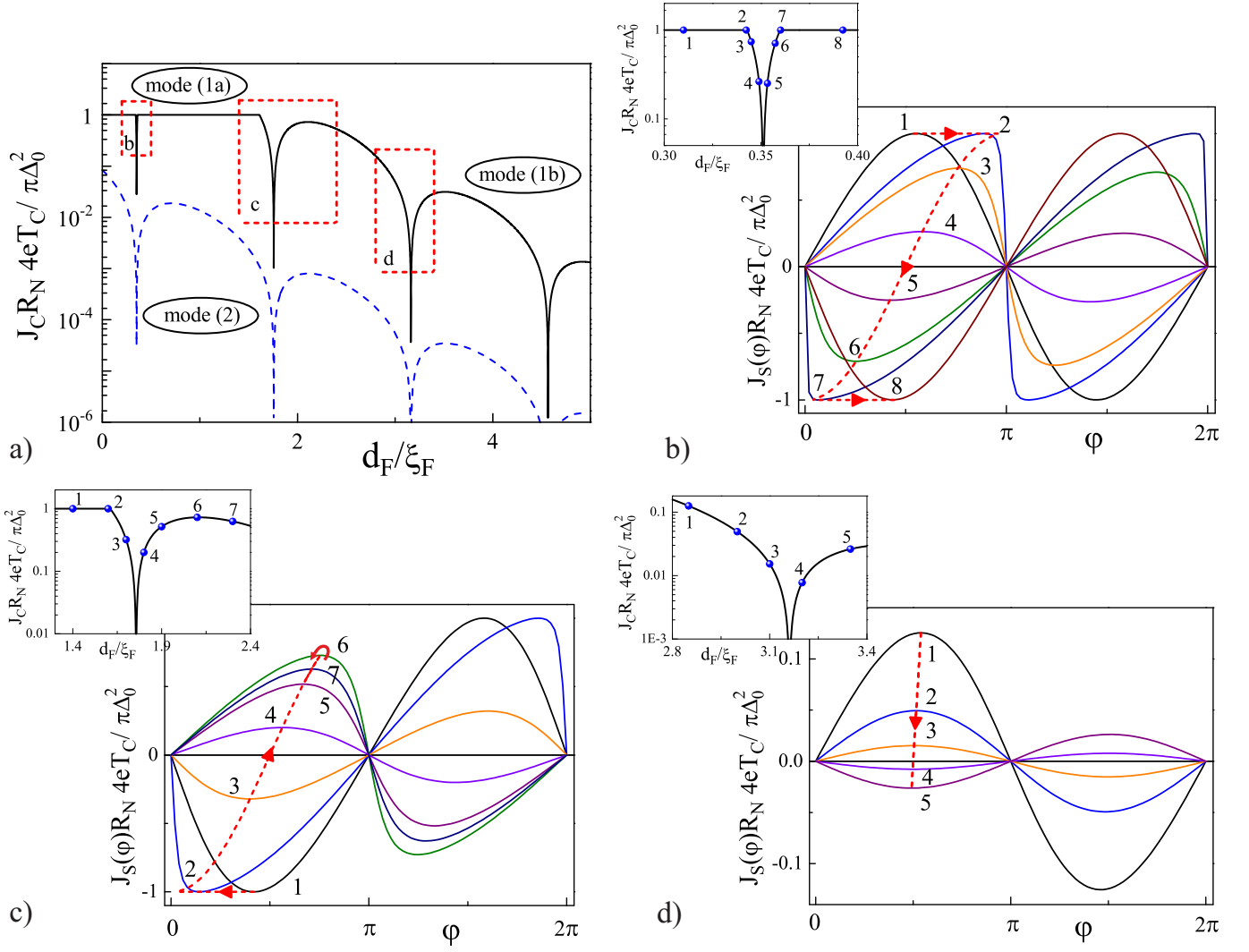


FIG. 4: a) Magnitude of the critical current  $J_C$  in the SISFS structure versus F-layer thickness  $d_F$  for two thickness of middle  $s$ -layer,  $d_s = 5\xi_s(T) > d_{sc}$  (solid line) and  $d_s = 0.5\xi_s(T) < d_{sc}$  (dashed line) calculated at  $T = 0.9T_C$  for  $H = 10\pi T_C$ ,  $\Gamma_{BI} = 200$  and  $\Gamma = 5$ . b)-d) CPR in the vicinity of  $0-\pi$  transitions. The corresponding insets show the enlarged parts of  $J_C(d_F)$  dependence enclosed in rectangles on the part a) of the Figure and marked by the letters b-d, respectively. The digits on the insets show the points at which the  $J_S(\varphi)$  curves have been calculated. The dashed lines in the Figs.4b-d are the loci of critical points at which the  $J_S(\varphi)$  dependence reaches its maximum value  $J_C(d_F)$ .

$d_F \gtrsim 1.6\xi_F$  there is a transition from *mode (1a)* to *mode (1b)*, which is accompanied by damped oscillation of  $J_C(d_F)$  with  $d_F$  increase.

### B. Mode (2): SINFS junction $d_s \leq d_{sc}$

For  $d_s \leq d_{sc}$  intrinsic superconductivity in the  $s$  layer is completely suppressed resulting in formation of the complex -InF- weak link area, where 'n' marks the intermediate  $s$  film in the normal state. In this parameter range the weak is always located in the tunnel barrier and the CPR has sinusoidal shape

$$J_S(\varphi) = \frac{J_G}{\sqrt{2}} \frac{(p-q) \sin \varphi}{2pq\Gamma\Gamma_{BI} \cos \frac{d_s}{\xi_s(T)} + [2pq\Gamma + (p+q)\Gamma_{BI}] \sin \frac{d_s}{\xi_s(T)}}. \quad (34)$$

In a vicinity of the critical thickness,  $d_s \lesssim d_{sc}$ , the factor  $\cos(d_s/\xi_s(T))$  in (34) is small and supercurrent is given by the expression

$$J_S(\varphi) = \frac{J_G}{2\sqrt{2}} \frac{(p-q) \sin \varphi}{2pq\Gamma + (p+q)\Gamma_{BI}}. \quad (35)$$

Further decrease of  $d_s$  into the limit  $d_s \ll d_{sc}$  leads to

$$J_S(\varphi) = \frac{J_G}{\sqrt{2}} \frac{(p-q) \sin \varphi}{2pq\Gamma\Gamma_{BI}}. \quad (36)$$

The magnitude of critical current in (36) is close to that in the well-known case of SIFS junctions in appropriate regime.

### C. Current-Phase Relation

In the previous section we have demonstrated that the variation in the thickness of the ferromagnetic layer should lead to the transformation of CPR of the SISFS structure. Fig.4a illustrates the  $J_C(d_F)$  dependencies calculated from expressions (23)-(28) at  $T = 0.9T_C$  for  $H = 10\pi T_C$ ,  $\gamma_B = 0$ ,  $\Gamma_{BI} \approx 200$  and  $\Gamma \approx 5$  for two thickness of the s layer  $d_s = 5\xi_S(T)$  (solid line) and  $d_s = 0.5\xi_S(T)$  (dashed line). In Figs.4b-d we enlarge the parts of  $J_C(d_F)$  dependence enclosed in rectangles labeled by letters b, c and d in Fig.4a and mark by digits the points where the  $J_S(\varphi)$  curves have been calculated. These curves are marked by the same digits as the points in the enlarge parts of  $J_C(d_F)$  dependencies. The dashed lines in the Figs.4b-d are the loci of critical points at which the  $J_S(\varphi)$  dependence reaches its maximum value,  $J_C(d_F)$ .

Figure 4b presents the *mode (1b)* valley, which divides the *mode (1a)* domain into 0- and  $\pi$ - states regions. In the *mode (1a)* domain the SISFS structure behaves as SIs and sFS junctions connected in series. Its critical current equals to the minimal one among the critical currents of the SIs ( $J_{CSIs}$ ) and sFS ( $J_{CsFS}$ ) parts of the device. In the considered case the thickness of the s film is sufficiently large to prevent suppression of superconductivity. Therefore,  $J_{CSIs}$  does not change when moving from the point 1 to the point 2 along  $J_C d_F$  dependence. At the point 2, when  $J_{CSIs} = J_{CsFS}$ , we arrive at the border between the *mode (1a)* and *mode (1b)*. It is seen that at this point there is maximum deviation of  $J_S(\varphi)$  from the sinusoidal shape. Further increase of  $d_F$  leads to 0- $\pi$  transition, when parameter  $\beta$  in (33) becomes small and  $J_S(\varphi)$  practically restores its sinusoidal shape. Beyond the area of 0 to  $\pi$  transition, the critical current changes its sign and CPR starts to deform again. The deformation achieves its maximum at the point 7 located at the other border between the *modes (1a)* and *(1b)*. The displacement from the point 7 to the point 8 along the  $J_C(d_F)$  dependence leads to recovery of sinusoidal CPR.

Figure 4c presents the transition from the  $\pi$ -state of *mode (1a)* to *mode (1b)* with  $d_F$  increase. It is seen that the offset from the point 1 to the points 2 – 5 along  $J_C(d_F)$  results in transformation of the CPR similar to that shown in Fig.4b during displacement in the direction from the point 1 to the points 2 – 6. The only difference is the starting negative sign of the critical current. However this behavior of CPR as well as close transition between modes lead to formation of the well pronounced kink at the  $J_C(d_F)$  dependence. Furthermore, contrary to Fig.4b at the point 6, the junction is still in the *mode (1b)* and remains in this mode with further increase in  $d_F$ . At the point 6 the critical current achieves its maximum value and it decreases along the dashed line for larger  $d_F$ .

Figure 4d shows the transformation of the CPR in the vicinity of the next 0 to  $\pi$  transition in *mode (1b)*. There is small deviation from sinusoidal shape at the point 1, which vanishes exponentially with an increase of  $d_F$ .

In the *mode (2)* (the dashed curve in Fig.4a) an intrinsic superconductivity in the s layer is completely suppressed resulting in the formation of a complex -InF- weak link region and the CPR becomes sinusoidal (34).

### IV. ARBITRARY TEMPERATURE

At arbitrary temperatures the boundary problem (2)-(11) goes beyond the assumptions of GL formalism and requires self-consistent solution. We have performed it numerically in terms of the nonlinear Usadel equations in iterative manner. All calculations were performed for  $T = 0.5T_C$ ,  $\xi_S = \xi_F$ ,  $\gamma_{BI} = 1000$ ,  $\gamma_{BFS} = 0.3$  and  $\gamma = 1$ .

Calculations show that at the selected transparency of tunnel barrier ( $\gamma_{BI} = 1000$ ) the suppression of superconductivity in the left electrode is negligibly small. This allows one to select the thickness of the left S electrode  $d_{SL} = 2\xi_S$  without any loss of generality. On the contrary, proximity of the right S electrode to the F layer results in strong suppression of superconductivity at the FS interface. Therefore the pair potential of the right S electrode reaches its bulk value only at thickness  $d_{SR} \gtrsim 10\xi_S$ . It is for these reasons we have chosen  $d_{SR} = 10\xi_S$  for the calculations.

Furthermore, the presence of a low-transparent tunnel barrier in the considered SISFS structures limits the magnitude of critical current  $J_C$  by a value much smaller compared to a depairing current of the superconducting electrodes. This allows one to neglect nonlinear corrections to coordinate dependence of the phase in the S banks.

The results of calculations are summarized in Fig.5. Figure 5a shows the dependence of  $J_C$  of the SISFS structure on the F-layer thickness  $d_F$  for relatively large  $d_s = 5\xi_S$  (solid) and small  $d_s = 0.5\xi_S$  (dashed) s-film thickness. The letters on the curves indicate the points at which the coordinate dependencies of the magnitude of the order parameter,  $|\Delta(x)|$ , and phase difference across the structure,  $\chi$ , have been calculated for the phase difference  $\varphi = \pi/2$ . These curves are shown in the panels b)-f) of the Fig.5 as the upper and bottom plots, respectively. There is direct correspondence between the letters, b, c, d, e, f, on  $J_C(d_F)$  curves and the labels, b), c), d), e), f), of the panels.

It is seen that qualitative behavior of the  $J_C(d_F)$  dependence at  $T = 0.5T_C$  remains similar to that obtained in the frame of the GL equations for  $T = 0.9T_C$  (see Fig.4a). Furthermore, the modes of operation discussed above remain relevant too. The panels b)-f) in Fig.5 make this statement more clear.

At the point marked by letter 'b', the s-film is sufficiently thick,  $d_s = 5\xi_S$ , while F film is rather thin,  $d_F = 0.3\xi_F$ , and therefore the structure is in 0- state of the *mode (1a)*. In this regime the phase mainly drops across the tunnel barrier, while the phase shifts at the s-film and in the S electrodes are negligibly small(see the bottom plot in Fig.5b).

At the point marked by the letter 'c' ( $d_s = 5\xi_S$ ,  $d_F = \xi_F$ ), the structure is in the  $\pi$ - state of the *mode (1a)*. It is seen from Fig.5c that there is a phase jump at the tunnel barrier and an additional  $\pi$ -shift occurs between the phases of S and s layers.

For  $d_F = 3\xi_F$  (Fig.5d) the position of the weak place shifts from SIs to sFS part of the SISFS junction. Then the structure starts to operate in the *mode (1b)*. It is seen that the phase drop across SIs part is small, while  $\varphi - \chi \approx \pi/2$  across the F layer, as it should be in SFS junctions with SIs and S electrodes.

At the points marked by the letters 'e' and 'f', thickness of the s-layer  $d_s = 0.5\xi_S$  is less than its critical value. Then su-

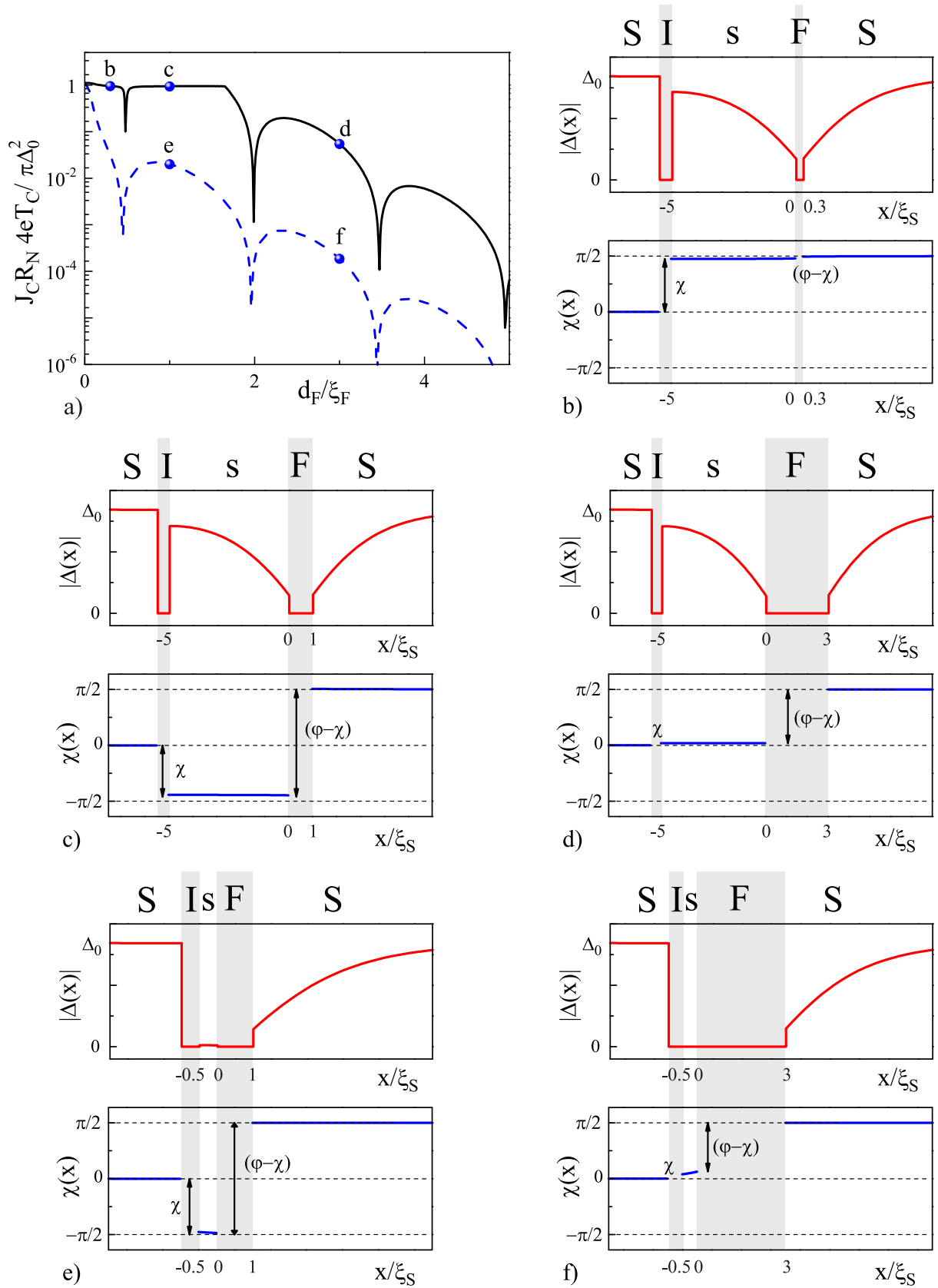


FIG. 5: a) Magnitude of critical current  $J_C$  of the SIsFS structure versus F-layer thickness  $d_F$  calculated at  $T = 0.5T_C$  for  $H = 10\pi T_C$ ,  $\gamma_{BI} = 1000$ ,  $\gamma = 1$  and two thickness of the s film  $d_s = 5\xi_S$  (solid line) and  $d_s = 0.5\xi_S$  (dashed line). The letters on  $J_C(d_F)$  give the points at which the coordinate dependencies of the magnitude of the order parameter,  $|\Delta(x)|$ , and phase difference across the structure,  $\chi$ , have been calculated. These curves are shown in the panels b)-f) of the Figure as the upper and bottom panels, respectively.

perconductivity in the s-spacer is suppressed due to the proximity with the F film and SISFS device operates in the *mode* (2). At  $d_F = \xi_F$  (the dot 'e' in Fig.5a and the panel Fig.5e) the position of the weak place is located at the SIs part of the structure and there is additional  $\pi$ -shift of phase across the F film. As a result, the SISFS structure behaves like an SInFS tunnel  $\pi$ -junction. Unsuppressed residual value of the pair potential is due to the proximity with the right S-electrode and it disappears with the growth of the F-layer thickness, which weakens this proximity effect. At  $d_F = 3\xi_F$  (Fig.5f) weak place is located at the F part of IsF trilayer. Despite strong suppression of the pair potential in the s-layer, the distribution of the phase inside the IsF weak place has rather complex structure, which depends on thicknesses of the s and F layers.

### A. Temperature crossover from 0 to $\pi$ states

The temperature-induced crossover from 0 to  $\pi$  states in SFS junctions has been discovered in<sup>26</sup> in structures with sinusoidal CPR. It was found that the transition takes place in a relatively broad temperature range.

Our analysis of SISFS structure (see Fig.6a) shows that smoothness of 0 to  $\pi$  transition strongly depends on the CPR shape. This phenomenon was not analyzed before since almost all previous theoretical results were obtained within a linear approximation leading in a sinusoidal CPR. To prove the statement, we have calculated numerically the set of  $J_C(T)$  curves for a number of F layer film thicknesses  $d_F$ . We have chosen the thickness of intermediate superconductor  $d_S = 5\xi_S$  in order to have SISFS device in the *mode*(1a) and we have examined the parameter range  $0.3\xi_F \leq d_F \leq \xi_F$ , in which the structure exhibits the first 0 to  $\pi$  transition. The borders of the  $d_F$  range are chosen in such a way that SISFS contact is either in 0- ( $d_F = 0.3\xi_F$ ) or  $\pi$ - ( $d_F = \xi_F$ ) state in the whole temperature range. The corresponding  $J_C(T)$  dependencies (dashed lines in Fig. 6a) provide the envelope of a set of  $J_C(T)$  curves calculated for the considered range of  $d_F$ . It is clearly seen that in the vicinity of  $T_C$  the decrease of  $d_F$  results in creation of the temperature range where 0-state exists. The point of 0 to  $\pi$  transition shifts to lower temperatures with decreasing  $d_F$ . For  $d_F \gtrsim 0.5\xi_F$  the transition is rather smooth since for  $T \geq 0.8T_C$  the junction keeps the *mode* (2) (with suppressed superconductivity) and deviations of the CPR from  $\sin(\varphi)$  are small. Thus the behavior of  $J_C(T)$  dependencies in this case can be easily described by analytic results from Sec.III C.

The situation drastically changes at  $d_F = 0.46\xi_F$  (short-dashed line in Fig.6a). For this thickness the point of 0 to  $\pi$  transition shifts to  $T \approx 0.25T_C$ . This shift is accompanied by an increase of amplitudes of higher harmonics of CPR (see Fig.6b). As a result, the shape of CPR is strongly modified, so that in the interval  $0 \leq \varphi \leq \pi$  the CPR curves are characterized by two values,  $J_{C1}$  and  $J_{C2}$ , as is known from the case of SFcFS constrictions<sup>41</sup>. In general,  $J_{C1}$  and  $J_{C2}$  differ both in sign and magnitude and  $J_C = \max(|J_{C1}|, |J_{C2}|)$ . For  $T > 0.25T_C$  the junction in the 0-state and  $J_C$  grows with decrease of  $T$  up to  $T \approx 0.5T_C$ . Further decrease of  $T$  is accompanied by suppression of critical current. In a vicinity of

$T \approx 0.25T_C$  the difference between  $|J_{C1}|$ , and  $|J_{C2}|$  becomes negligible and the system starts to develop the instability that eventually shows up as a sharp jump from 0 to  $\pi$  state. After the jump,  $|J_C|$  continuously increases when  $T$  goes to zero.

It is important to note that this behavior should always be observed in the vicinity of 0 –  $\pi$  transition, i.e. in the range of parameters, in which the amplitude of the first harmonic is small compared to higher harmonics. However, the closer is temperature to  $T_C$ , the less pronounced are higher CPR harmonics and the smaller is the magnitude of the jump. This fact is illustrated by dash-dotted line showing  $J_C(T)$  calculated for  $d_F = 0.48\xi_F$ . The jump in the curves calculated for  $d_F \geq 0.5\xi_F$  also exists, but it is small and can not be resolved on the scale used in the Fig. 6a.

At  $d_F = 0.45\xi_F$  (dash-dot-dotted line in Fig. 6) the junction is always in the 0-state and there is only small suppression of critical current at low temperatures despite the realization of non-sinusoidal CPR.

Thus the calculations clearly show that it's possible to realize a set of parameters of SISFS junctions where thermally-induced 0- $\pi$  crossover can be observed and controlled by temperature variation.

### B. 0 to $\pi$ crossover by changing the effective exchange energy in external magnetic field

Exchange field is an intrinsic microscopic parameter of a ferromagnetic material which cannot be controlled directly by application of an external field. However, the spin splitting in F-layers can be provided by both the internal exchange field and external magnetic field<sup>42,43</sup>, resulting in generation of effective exchange field, which equals to their sum. However, practical realization of this effect is a challenge since it is difficult to fulfill special requirements<sup>42,43</sup> on thickness of S electrodes and SFS junction geometry.

Another opportunity can be realized in soft diluted ferromagnetic alloys like  $\text{Fe}_{0.01}\text{Pd}_{0.99}$ . Investigations of magnetic properties<sup>44</sup> of these materials have shown that below 14 K they exhibit ferromagnetic order due to the formation of weakly coupled ferromagnetic nanoclusters. In the clusters, the effective spin polarization of Fe ions is about  $4\mu_B$ , corresponding to that in the bulk  $\text{Pd}_3\text{Fe}$  alloy. It was demonstrated that the hysteresis loops of  $\text{Fe}_{0.01}\text{Pd}_{0.99}$  films have the form typical to nanostructured ferromagnets with weakly coupled grains (the absence of domains; a small coercive force; a small interval of the magnetization reversal, where the magnetization changes its direction following the changes in the applied magnetic field; and a prolonged part, where the component of the magnetization vector along the applied field grows gradually).

Smallness of concentration of  $\text{Pd}_3\text{Fe}$  clusters and their ability to follow variation in the applied magnetic field may result in generation of  $H_{eff}$ , which is of the order of

$$H_{eff} \approx H \frac{n_{\uparrow}V_{\uparrow} - n_{\downarrow}V_{\downarrow}}{n_{\downarrow}V_{\downarrow} + n_{\uparrow}V_{\uparrow} + (n - n_{\uparrow} - n_{\downarrow})(V - V_{\downarrow} - V_{\uparrow})}. \quad (37)$$

Here  $n$  is concentration of electrons within a physically small

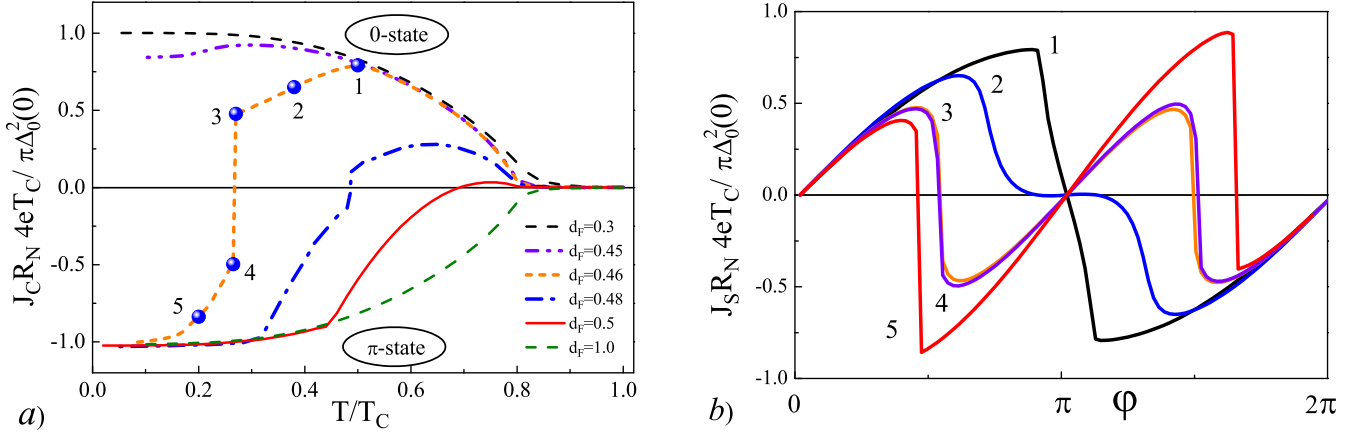


FIG. 6: a) Critical current  $J_C$  of the SISFS structure versus temperature  $T$  for various F-layer thicknesses  $d_F$  in the vicinity of 0 to  $\pi$  transition. Dashed envelopes show temperature dependence in the 0- (top) and  $\pi$ - (bottom) states. b) CPR of the structure with  $d_F = 0.46\xi_F$  for a set of the temperatures in the vicinity of 0-  $\pi$  transition. Each curve corresponds to the point marked in the panel (a). Note that the curves (3) and (4) almost coincide but correspond to different ground states of the junction, 0- and  $\pi$ , respectively. The calculations have been performed numerically for  $d_s = 5\xi_S$ ,  $H = 10\pi T_C$ ,  $\gamma_{BI} = 1000$ ,  $\gamma_B = 0.3$ ,  $\gamma = 1$ .

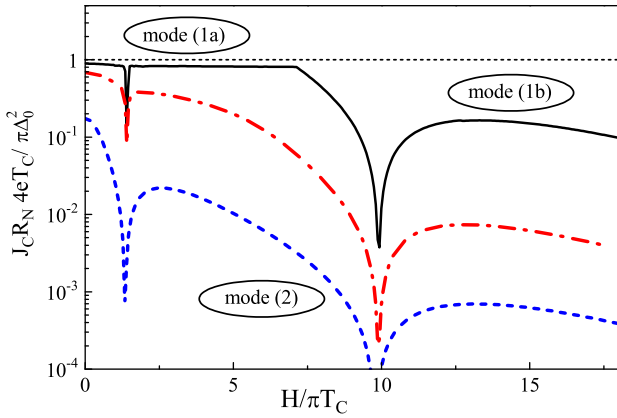


FIG. 7: The magnitude of critical current  $J_C$  of the SISFS structure versus exchange field  $H$  for thick  $d_s = 5\xi_S$  (solid), thin  $d_s = 0.5\xi_S$  (dashed) and intermediate  $d_s = 3\xi_S$  (dash-dotted) s-layer thickness. The plot demonstrates the possibility of 0- $\pi$  transition by varying the effective exchange field. The calculations have been performed for  $T = 0.5T_C$ ,  $d_F = 2\xi_F$ ,  $\gamma_{BI} = 1000$ ,  $\gamma_B = 0.3$ ,  $\gamma = 1$ .

volume  $V$ , in which one performs an averaging of Greens functions in the transformation to a quasiclassical description of superconductivity,  $n_{\uparrow,\downarrow}$  and  $V_{\uparrow,\downarrow}$  are the values describing spin polarized parts of  $n$  and parts of volume  $V$ , which they occupy, respectively. Similar kind of  $H_{eff}$  nucleates in NF or SF proximity structures, which are composed from thin layers<sup>45-48</sup>. There is an interval of applied magnetic fields  $H_{ext}$  where the alloy magnetization changes its direction and the concentrations  $n_{\uparrow,\downarrow}$  depend on a pre-history of application of the field<sup>10,12</sup>, providing the possibility to control  $H_{eff}$  by an external magnetic field.

Derivation of possible relationships between  $H_{eff}$  and  $H_{ext}$

is outside of the scope of this paper. Below we will concentrate only on an assessment of the intervals in which  $H_{eff}$  should be changed to ensure the transition of SISFS device from 0 to  $\pi$  state. To do this, we calculate the  $J_C(H)$  dependencies presented in Fig.7. The calculations have been done for the set of structures with  $d_F = 2\xi_F$  and s-films thickness ranging from thick one,  $d_s = 5\xi_S$  (solid line) up to an intermediate value  $d_s = 2\xi_S$  (dashed-dotted line) and finishing with thin film having  $d_s = 0.5\xi_S$  (dashed line). It is clearly seen that these curves have the same shape as  $J_C(d_F)$  dependencies presented in the Sec.III. For  $d_s = 5\xi_S$  and  $H \lesssim 7\pi T_C$  the magnitude of  $J_C$  is practically independent on  $H$ , but it changes the sign at  $H \approx 1.25\pi T_C$  due to 0 -  $\pi$  transition. It is seen that for the transition, while maintaining the normalized current value at a level close to unity, changes of  $H$  are required approximately of the order of  $0.1\pi T_C$  or 10%. For  $d_s = 2\xi_S$  and  $H \lesssim 3\pi T_C$ , it is necessary to change  $H$  on 20% to realize the such a transition. In this case the value of normalized current is at the level 0.4. In mode 2 the transition requires 100% change of  $H$ , which is not practical.

## V. DISCUSSION

We have performed a theoretical study of magnetic SISFS Josephson junctions. At  $T \leq T_C$  calculations have been performed analytically in the frame of the GL equations. For arbitrary temperatures we have developed numerical code for selfconsistent solution of the Usadel equations. We have outlined several modes of operation of these junctions. For s-layer in superconducting state they are S-I-sfS or SIS-F-S devices with weak place located at insulator (*mode (1a)*) and at the F-layer (*mode (1b)*), respectively. For small s-layer thickness, intrinsic superconductivity in it is completely suppressed resulting in formation of InF weak place (*mode (2)*). We have examined the shape of  $J_S(\varphi)$  and spatial distribution of the

module of the pair potential and its phase difference across the SISFS structure in these modes.

For *mode (1)* the shape of the CPR can substantially differ from the sinusoidal one even in a vicinity of  $T_C$ . The deviations are largest when the structure is close to the crossover between the *modes (1a)* and *(1b)*. This effect results in the kinks in the dependencies of  $J_C$  on temperature and on parameters of the structure (thickness of the layers  $d_F$ ,  $d_S$  and exchange energy  $H$ ) as illustrated in Fig.4 on  $J_C(d_F)$  curves. The transformation of CPR is even more important at low temperatures. For  $T \lesssim 0.25T_C$  a sharp  $0 - \pi$  transition can be realized induced by small temperature variation (Fig.6). This instability must be taken into account when using the structures as memory elements. On the other hand, this effect can be used in detectors of electromagnetic radiation, where absorption of a photon in the F layer will provide local heating leading to development of the instability and subsequent phonon registration.

We have shown that suppression of the order parameter in the thin s-film due to the proximity effect leads to decrease of  $J_C R_N$  product in both  $0-$  and  $\pi-$  states. On the other hand, the proximity effect may also support s-layer superconductivity due to the impact of S electrodes. In *mode (1a)*  $J_C R_N$  product in  $0-$  and  $\pi-$  states can achieve values typical for SIS tunnel junctions.

In *mode (2)* sinusoidal CPR is realized. Despite that, the distribution of the phase difference  $\chi(x)$  in the IsF weak place may have a complex structure, which depends on thickness of the s and F layers. These effects should influence the dynamics of a junction in its *ac*-state and deserve further study.

Further, we have also shown that in *mode (1a)* nearly 10% change in the exchange energy can cause a  $0 - \pi$  transition, i.e. changing the sign of  $J_C R_N$  product, while maintaining its absolute value. This unique feature can be implemented in *mode (1a)*, since it is in it changes of the exchange energy only determine the presence or absence of a  $\pi$  shift between s and S electrodes and does not affect the magnitude of the critical current of SIS part of SISFS junction.

In *mode (1b)*, the F layer becomes a part of weak link area. In this case the  $\pi$  shift, initiated by the change in  $H$  must be accompanied by changes of  $J_C$  magnitude due to the oscillatory nature of superconducting correlations in the F film. The latter may lead to very complex and irregular dependence of  $J_C(H_{ext})$ , which have been observed in Nb-PdFe-Nb SFS junctions (see Fig.3 in<sup>8</sup>). Contrary to that the  $J_C(H_{ext})$  curves of SISFS structure with the same PdFe metal does not demonstrate these irregularities<sup>10,11</sup>.

To characterize a junction stability with respect to  $H$  variations it is convenient to introduce the parameter  $\eta = (dJ_C/J_C)/(dH/H)$  which relates the relative change in the critical current to the relative change in the exchange energy. The larger the magnitude of  $\eta$  the more intensive irregularities in an SFS junction are expected with variation of  $H$ . In the Fig.8 we compare the SISFS devices with conventional SFS, SIFS and SIFIS junctions making use of two the most important parameters: the instability parameter  $\eta$  and  $J_C R_N$  product, the value, which characterizes high frequency properties of the structures. The calculations have been done in the

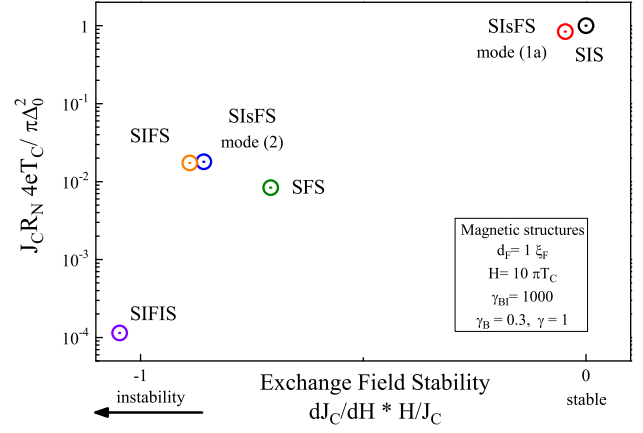


FIG. 8: Comparison of different types of Josephson structures, marked by points on the phase plane, in terms of  $J_C R_N$  and exchange field stability  $\eta$ . All calculation have been performed for  $T = 0.5T_C$ ,  $d_F = \xi_F$ ,  $\gamma_{BI} = 1000$ ,  $\gamma_B = 0.3$ ,  $\gamma = 1$ . For SISFS structures  $d_S = 5\xi_S$  and  $d_S = 0.5\xi_S$  are taken in *mode (1a)* and *mode (2)*, respectively.

frame of Usadel equation for the same set of junctions parameters, namely  $T = 0.5T_C$ ,  $H = 10\pi T_C$ ,  $d_F = \xi_F$ ,  $\gamma_{BI} = 1000$ ,  $\gamma_B = 0.3$ ,  $\gamma = 1$ .

It can be seen that the presence of two tunnel barriers in SIFIS junction results in the smallest  $J_C R_N$  and strong instability. The SIFS and SISFS structures in the *mode (2)* demonstrate better results with almost the same parameters. Conventional SFS structures have two times smaller  $J_C R_N$  product, having higher critical current but lower resistivity. At the same time, SFS junctions are more stable due to the lack of low-transparent tunnel barrier. The latter is the main source of instability due to sharp phase discontinuities at the barrier 'I'.

Contrary to the standard SFS, SIFS and SIFIS junctions, SISFS structures achieve  $J_C R_N$  and stability characteristics comparable to those of SIS tunnel junctions. This unique property is favorable for application of SISFS structures in superconducting electronic circuits.

### Acknowledgments

We thank V.V. Ryazanov, V.V. Bol'ginov, I.V. Vernik and O.A. Mukhanov for useful discussions. This work was supported by the Russian Foundation for Basic Research, Russian Ministry of Education and Science, Dynasty Foundation, Scholarship of the President of the Russian Federation, IARPA and Dutch FOM.

### Appendix A: Boundary problem at $T \lesssim T_C$

In the limit of high temperature

$$G_S = G_s = G_F = \text{sgn}(\Omega) \quad (\text{A1})$$

and the boundary problem reduces to the system of linearized equations. Their solution in the F layer, ( $0 \leq x \leq d_F$ ), has the form

$$\Phi_F = C \sinh \frac{\sqrt{\Theta}(x - d_F/2)}{\xi_F} + D \cosh \frac{\sqrt{\Theta}(x - d_F/2)}{\xi_F}, \quad (\text{A2})$$

where  $\Theta = \tilde{\Omega} \text{sgn}(\Omega)$ . For transparent FS and sF interfaces ( $\gamma_B = 0$ ) from the boundary conditions (6), (7) and (A2) it is easy to get that

$$\frac{\xi_S}{\gamma\sqrt{\Theta}} \frac{d}{dx} \Phi_s(0) = -\Phi_s(0) \coth \frac{d_F \sqrt{\Theta}}{\xi_F} + \frac{\Phi_S(d_F)}{\sinh \frac{d_F \sqrt{\Theta}}{\xi_F}}, \quad (\text{A3})$$

$$\frac{\xi_S}{\gamma\sqrt{\Theta}} \frac{d}{dx} \Phi_S(d_F) = \Phi_S(d_F) \coth \frac{d_F \sqrt{\Theta}}{\xi_F} - \frac{\Phi_s(0)}{\sinh \frac{d_F \sqrt{\Theta}}{\xi_F}}. \quad (\text{A4})$$

and thus reduce the problem to the solution of Ginzburg-Landau (GL) equations in s and S films.

$$\xi_S^2(T) \frac{d^2}{dx^2} \Delta_k - \Delta_k (\Delta_0^2 - |\Delta_k|^2) = 0, \quad \Delta_0^2 = \frac{8\pi^2 T_C (T_C - T)}{7\zeta(3)}, \quad (\text{A5})$$

$$J = \frac{J_G}{\Delta_0^2} \text{Im} \left( \Delta_k^* \xi_S(T) \frac{d}{dx} \Delta_k \right), \quad J_G = \frac{\pi \Delta_0^2}{4e\rho_s T_C \xi_S(T)}, \quad (\text{A6})$$

where  $\xi_S(T) = \pi \xi_S / 2 \sqrt{1 - T/T_C}$  is GL coherence length and  $k$  equals to  $s$  or  $S$  for  $-d_s \leq x \leq 0$  and  $x \geq d_F$ , respectively. At Is, sF and FS interfaces GL equations should be supplemented by the boundary conditions in the form<sup>37</sup>

$$\xi_S(T) \frac{d}{dx} \Delta_k(z) = b(z) \Delta_k(z), \quad b(z) = \frac{\Sigma_1(z)}{\Sigma_2(z)}, \quad (\text{A7})$$

$$\Sigma_1(z) = \sum_{\omega=-\infty}^{\infty} \xi_S(T) \frac{d}{dx} \frac{\Phi_k(z)}{\Omega^2}, \quad \Sigma_2(z) = \sum_{\omega=-\infty}^{\infty} \frac{\Phi_k(z)}{\Omega^2}, \quad (\text{A8})$$

where  $z = -d_s, 0, d_F$ . In typical experimental situation  $\gamma_{BI} \gg 1$ ,  $\gamma\sqrt{H} \gg 1$  and  $d_F \sqrt{H} \gtrsim \xi_F$ . In this case in the first approximation

$$\Phi_S(d_F) = 0, \quad \Phi_s(0) = 0, \quad \frac{d}{dx} \Phi_s(-d_s) = 0$$

and in the vicinity of interfaces

$$\Phi_S(x) = \Delta_S(x) = B_S \frac{(x - d_F)}{\xi_S(T)}, \quad d_F \lesssim x \ll \xi_S(T), \quad (\text{A9})$$

$$\Phi_s(x) = \Delta_s(x) = -B_S \frac{x}{\xi_S(T)}, \quad -\xi_S(T) \ll x \lesssim 0, \quad (\text{A10})$$

$$\Phi_s(x) = \Delta_s(x) = \Delta_s(-d_s), \quad -d_s \lesssim x \ll -d_s + \xi_S(T), \quad (\text{A11})$$

where  $B_S$ ,  $B_s$ , and  $\Delta_s(-d_s)$  are independent on  $x$  constants. Substitution of the solutions (A9) - (A11) into (15), (A3), (A4) gives

$$\Gamma_{BI} \xi_S(T) \frac{d}{dx} \Phi_s(-d_s) = \Delta_s(-d_s) - \Delta_0, \quad (\text{A12})$$

$$\Phi_S(d_F) = \frac{B_S}{\Gamma \sqrt{\Theta} \sinh \frac{d_F \sqrt{\Theta}}{\xi_F}} + \frac{B_S \cosh \frac{d_F \sqrt{\Theta}}{\xi_F}}{\Gamma \sqrt{\Theta} \sinh \frac{d_F \sqrt{\Theta}}{\xi_F}}, \quad (\text{A13})$$

$$\Phi_s(0) = \frac{B_s \cosh \frac{d_F \sqrt{\Theta}}{\xi_F}}{\Gamma \sqrt{\Omega} \sinh \frac{d_F \sqrt{\Theta}}{\xi_F}} + \frac{B_S}{\Gamma \sqrt{\Theta} \sinh \frac{d_F \sqrt{\Theta}}{\xi_F}}, \quad (\text{A14})$$

$$\Gamma_{BI} = \frac{\gamma_{BI} \xi_S}{\xi_S(T)}, \quad \Gamma = \frac{\gamma_{BI} \xi_S(T)}{\xi_S}. \quad (\text{A15})$$

From definition (A7), (A8) of coefficients  $b(z)$  and expressions (A12) - (A14) it follows that

$$\Gamma_{BI} \xi_S(T) \frac{d}{dx} \Delta_s(-d_s) = -(\Delta_0 - \Delta_s(-d_s)), \quad (\text{A16})$$

$$\xi_S(T) \frac{d}{dx} \Delta_s(0) = -\frac{q+p}{2} \Gamma \Delta_s(0) - \frac{q-p}{2} \Gamma \Delta_S(d_F), \quad (\text{A17})$$

$$\xi_S(T) \frac{d}{dx} \Delta_S(d_F) = \frac{q+p}{2} \Gamma \Delta_S(d_F) + \frac{q-p}{2} \Gamma \Delta_s(0), \quad (\text{A18})$$

where

$$p^{-1} = \frac{8}{\pi^2} \text{Re} \sum_{\omega=0}^{\infty} \frac{1}{\Omega^2 \sqrt{\Omega} \coth \frac{d_F \sqrt{\Omega}}{2\xi_F}}, \quad (\text{A19})$$

$$q^{-1} = \frac{8}{\pi^2} \text{Re} \sum_{\omega=0}^{\infty} \frac{1}{\Omega^2 \sqrt{\Omega} \tanh \frac{d_F \sqrt{\Omega}}{2\xi_F}}. \quad (\text{A20})$$

In considered limit both suppression parameters  $\Gamma_{BI} \gg 1$  and  $\Gamma \gg 1$  are large and from relations (15), (A3), (A4) in the first approximation on these parameters we get that the boundary conditions (A16) - (A18) can be simplified to

$$\xi_S(T) \frac{d}{dx} \Delta_s(-d_s) = 0, \quad \Delta_s(0) = 0, \quad \Delta_S(d_F) = 0. \quad (\text{A21})$$

Taking into account that in this approximation supercurrent  $j = 0$  and  $\Delta_S(\infty) = \Delta_0$  from (A5), (A21) it follows that

$$\Delta_S(x) = \delta_S(x) \exp\{i\varphi\}, \quad \delta_S(x) = \Delta_0 \tanh \frac{x - d_F}{\sqrt{2}\xi_S(T)}, \quad (\text{A22})$$

while

$$\Delta_s(x) = \delta_s(x) \exp\{i\chi\}, \quad (\text{A23})$$

where  $\delta_s(x)$  is the solution of transcendental equation

$$F\left(\frac{\delta_s(x)}{\delta_s(-d_s)}, \frac{\delta_s(-d_s)}{\Delta_0\eta}\right) = -\frac{x\eta}{\sqrt{2}\xi_s(T)}, \quad \eta = \sqrt{2 - \frac{\delta_s^2(-d_s)}{\Delta_0^2}} \quad (\text{A24})$$

and  $\delta_s(-d_s)$  is a solution of the same equation at the SIs boundary  $x = -d_s$

$$K\left(\frac{\delta_s(-d_s)}{\Delta_0\eta}\right) = \frac{d_s\eta}{\sqrt{2}\xi_s(T)}. \quad (\text{A25})$$

Here  $F(y, z)$  and  $K(z)$  are the incomplete and complete elliptic integral of the first kind respectively.

Substitution of (A22), (A23) into (A16) - (A18) gives that in the next approximation on  $\Gamma_{BI}^{-1}$  and  $\Gamma^{-1}$

$$J(-d_s) = J_G \frac{\delta_s(-d_s)}{\Gamma_{BI}\Delta_0} \sin(\chi) \quad (\text{A26})$$

$$J(0) = J(d_F) = J_G \frac{\Gamma(p-q)}{2\Delta_0^2} \delta_s(0)\delta_s(d_F) \sin(\varphi - \chi), \quad (\text{A27})$$

where

$$\delta_s(0) = -\frac{2b(q-p)\cos(\varphi - \chi) + 2a(q+p)}{\Gamma\left[(q+p)^2 - (q-p)^2\cos^2(\varphi - \chi)\right]}, \quad (\text{A28})$$

$$\delta_s(d_F) = \frac{2b(q+p) + 2a(q-p)\cos(\varphi - \chi)}{\Gamma\left[(q+p)^2 - (q-p)^2\cos^2(\varphi - \chi)\right]}, \quad (\text{A29})$$

are magnitudes of the order parameters at the FS interfaces and

$$a = -\delta_s(-d_s)\sqrt{1 - \frac{\delta_s^2(-d_s)}{2\Delta_0^2}}, \quad b = \frac{\Delta_0}{\sqrt{2}} \quad (\text{A30})$$

Phase,  $\chi$ , of the order parameters of the s layer is determined from equality of currents (A26), (A27).

- 
- <sup>1</sup> A. A. Golubov, M. Yu. Kupriyanov, E. Il'ichev, Rev. Mod. Phys. **76**, 411 (2004).
  - <sup>2</sup> A. I. Buzdin, Rev. Mod. Phys. **77**, 935 (2005).
  - <sup>3</sup> F. S. Bergeret, A. F. Volkov, K. B. Efetov, Rev. Mod. Phys. **77**, 1321 (2005).
  - <sup>4</sup> S. Oh, D. Youm, and M. Beasley, Appl. Phys. Lett. **71** 2376, (1997).
  - <sup>5</sup> R. Held, J. Xu, A. Schmehl, C.W. Schneider, J. Mannhart, and M. Beasley, Appl. Phys. Lett. **89**, 163509 (2006).
  - <sup>6</sup> C. Bell, G. Burnell, C. W. Leung, E. J. Tarte, D.-J. Kang, and M. G. Blamire, Appl. Phys. Lett. **84**, 1153 (2004).
  - <sup>7</sup> E. Goldobin, H. Sickinger, M. Weides, N. Ruppelt, H. Kohlstedt, R. Kleiner, D. Koelle, arXiv:1306.1683 (2013).
  - <sup>8</sup> V. V. Bol'ginov, V. S. Stolyarov, D. S. Sobanin, A. L. Karpovich, and V. V. Ryazanov, Pis'ma v ZhETF **95**, 408 (2012) [JETP Lett. **95** 366 (2012)].
  - <sup>9</sup> V. V. Ryazanov, V. V. Bol'ginov, D. S. Sobanin, I. V. Vernik, S. K. Tolpygo, A. M. Kadin, O. A. Mukhanov, Physics Procedia **36**, 35 (2012).
  - <sup>10</sup> T. I. Larkin, V. V. Bol'ginov, V. S. Stolyarov, V. V. Ryazanov, I. V. Vernik, S. K. Tolpygo, and O. A. Mukhanov, Appl. Phys. Lett. **100**, 222601 (2012).
  - <sup>11</sup> I. V. Vernik, V. V. Bol'ginov, S. V. Bakurskiy, A. A. Golubov, M. Yu. Kupriyanov, V. V. Ryazanov and O. A. Mukhanov, IEEE Tran. Appl. Supercond., **23**, 1701208 (2013).
  - <sup>12</sup> S. V. Bakurskiy, N. V. Klenov, I. I. Soloviev, V. V. Bol'ginov, V. V. Ryazanov, I. I. Vernik, O. A. Mukhanov, M. Yu. Kupriyanov, and A. A. Golubov, Appl. Phys. Lett. **102**, 192603 (2013).
  - <sup>13</sup> T. Orllepp, Ariando, O. Mielke, C. J. M. Verwijs, K. F. K. Foo, H. Rogalla, F. H. Uhlmann, and H. Hilgenkamp, Science **312**, 1495 (2006).
  - <sup>14</sup> V. Ryazanov, Uspechi Fizicheskich Nauk **169**, 920 (1999) [Physics-Uspekhi **42**, 825 (1999)].
  - <sup>15</sup> A.K. Feofanov, V.A. Oboznov, V.V. Bol'ginov, *et. al.*, Nature Physics **6**, 593 (2010).
  - <sup>16</sup> A. V. Ustinov and V. K. Kaplunenko, J. Appl. Phys. **94**, 5405 (2003).
  - <sup>17</sup> A. Buzdin and A. E. Koshelev, Phys. Rev. B **67**, 220504(R) (2003).
  - <sup>18</sup> A. E. Koshelev, Phys. Rev. B **86**, 214502 (2012).
  - <sup>19</sup> N. G. Pugach, E. Goldobin, R. Kleiner, and D. Koelle, Phys. Rev. B **81**, 104513 (2010).
  - <sup>20</sup> E. Goldobin, D. Koelle, R. Kleiner, and R.G. Mints, Phys. Rev. Lett, **107**, 227001 (2011).
  - <sup>21</sup> H. Sickinger, A. Lipman, M Weides, R.G. Mints, H. Kohlstedt, D. Koelle, R. Kleiner, and E. Goldobin, Phys. Rev. Lett, **109**, 107002 (2012).
  - <sup>22</sup> S. V. Bakurskiy, N. V. Klenov, T. Yu. Karminskaya, M. Yu. Kupriyanov, and A. A. Golubov, Supercond. Sci. Technol. **26**, 015005 (2013).
  - <sup>23</sup> D. M. Heim, N. G. Pugach, M. Yu. Kupriyanov, E. Goldobin, D. Koelle, and R. Kleiner, J. Phys. Cond. Mat. **25**, 215701 (2013).
  - <sup>24</sup> M. Alidoust, J. Linder, Phys. Rev. B **87**, 060503 (2013).
  - <sup>25</sup> Jun-Feng Liu, K.S. Chan, Phys. Rev. B **82**, 184533 (2010).
  - <sup>26</sup> V. V. Ryazanov, V. A. Oboznov, A. Yu. Rusanov, A. V. Veretennikov, A. A. Golubov, and J. Aarts, Phys. Rev. Lett. **86**, 2427 (2001).
  - <sup>27</sup> V. A. Oboznov, V. V. Bol'ginov, A. K. Feofanov, V. V. Ryazanov, and A. I. Buzdin, Phys. Rev. Lett. **96**, 197003 (2006).
  - <sup>28</sup> T. Kontos, M. Aprili, J. Lesueur, F. Genet, B. Stephanidis, and R. Boursier, Phys. Rev. Lett. **89**, 137007 (2002).
  - <sup>29</sup> M. Weides, M. Kemmler, H. Kohlstedt, A. Buzdin, E. Goldobin, D. Koelle, R. Kleiner, Appl. Phys. Lett. **89**, 122511 (2006).
  - <sup>30</sup> M. Weides, M. Kemmler, H. Kohlstedt, R. Waser, D. Koelle, R. Kleiner, and E. Goldobin Physical Review Letters **97**, 247001 (2006).
  - <sup>31</sup> F. Born, M. Siegel, E. K. Hollmann, H. Braak, A. A. Golubov, D. Yu. Gusakova, and M. Yu. Kupriyanov, Phys. Rev. B. **74**, 140501 (2006).
  - <sup>32</sup> J. Pfeiffer, M. Kemmler, D. Koelle, R. Kleiner, E. Goldobin, M. Weides, A. K. Feofanov, J. Lisenfeld, and A. V. Ustinov, Physical Review B **77**, 214506 (2008).

- <sup>33</sup> A. S. Vasenko, A. A. Golubov, M. Yu. Kupriyanov, and M. Weides, *Phys.Rev.B*, **77**, 134507 (2008).
- <sup>34</sup> A. S. Vasenko, S. Kawabata, A. A. Golubov, M. Yu. Kupriyanov, C. Lacroix, F. W. J. Hekking, *Phys. Rev. B* **84**, 024524 (2011).
- <sup>35</sup> K. D. Usadel, *Phys. Rev. Lett.* **25**, 507 (1970).
- <sup>36</sup> M. Yu. Kupriyanov and V. F. Lukichev, *Zh. Eksp. Teor. Fiz.* **94**, 139 (1988) [*Sov. Phys. JETP* **67**, 1163 (1988)].
- <sup>37</sup> Z. G.Ivanov, M. Yu. Kupriyanov, K. K. Likharev, S. V. Meriakri, and O. V. Snigirev, *Fiz. Nizk. Temp.* **7**, 560 (1981). [*Sov. J. Low Temp. Phys.* **7**, 274 (1981)].
- <sup>38</sup> A. A.Zubkov, and M. Yu. Kupriyanov, *Fiz. Nizk. Temp.* **9**, 548 (1983) [*Sov. J. Low Temp. Phys.* **9**, 279 (1983)].
- <sup>39</sup> M. Yu. Kupriyanov, *Pis'ma v ZhETF* **56**, 414 (1992) [*JETP Lett.* **56**, 399 (1992)].
- <sup>40</sup> A.A. Golubov and M.Y. Kupriyanov, *Pis'ma v ZhETF* **81**, 419 (2005) [*JETP Lett.* **81**, 335 (2005)].
- <sup>41</sup> A.A. Golubov, M.Y. Kupriyanov, and Y.V. Fominov, *Pis'ma v ZhETF* **75**, 709 (2002). [*JETP Lett.* **75**, 588 (2002)].
- <sup>42</sup> R. Meservey and P. M. Tedrow, *Phys. Rep.* **238**, 173 (1994).
- <sup>43</sup> E. A. Koshina, V. N. Krivoruchko, *Metallofizika i Noveishie Tekhnologii*, **35**, 45 (2013).
- <sup>44</sup> L. S. Uspenskaya, A. L. Rakhmanov, L. A. Dorosinskiy, A. A. Chugunov, V. S. Stolyarov, O. V. Skryabina, and S. V. Egorov, *Pis'ma v ZhETF* **97**, 176 (2013) [*JETP Lett.* **97**, 155 (2013)].
- <sup>45</sup> F. S. Bergeret, A. F. Volkov, and K. B. Efetov, *Phys. Rev.Lett.* **86**, 3140 (2001).
- <sup>46</sup> Ya. V. Fominov, N. M. Chtchelkatchev, and A. A. Golubov, *Phys. Rev. B* **66**, 014507 (2002).
- <sup>47</sup> T. Yu. Karminskaya and M. Yu. Kupriyanov, *Pis'ma v ZhETF* **85**, 343 (2007) [*JETP Lett.* **85**, 286 (2007)].
- <sup>48</sup> T. E. Golikova, F. Hübler, D. Beckmann, I. E. Batov, T. Yu. Karminskaya, M. Yu. Kupriyanov, A. A. Golubov and V. V. Ryazanov, *Phys. Rev. B* **86**, 064416 (2012).